Aerogels Hot Paper

Deutsche Ausgabe: DOI: 10.1002/ange.201605510
Internationale Ausgabe: DOI: 10.1002/anie.201605510

Polymerization under Hypersaline Conditions: A Robust Route to Phenolic Polymer-Derived Carbon Aerogels

Zhi-Long Yu, Guan-Cheng Li, Nina Fechler, Ning Yang, Zhi-Yuan Ma, Xin Wang, Markus Antonietti,* and Shu-Hong Yu**

Abstract: *Polymer-derived carbon aerogels can be obtained by direct polymerization of monomers under hypersaline conditions using inorganic salts. This allows for significantly increased mechanical robustness and avoiding special drying processes. This concept was realized by conducting the polymerization of phenol–formaldehyde (PF) in the presence of $ZnCl_2$ salt. Afterwards, the simultaneous carbonization and foaming process conveniently converts the PF monolith into a foam-like carbon aerogel. $ZnCl_2$ plays a key role, serving as dehydration agent, foaming agent, and porogen. The carbon aerogels thus obtained are of very low density (25 mg cm^{-3}), high specific surface area (1340 m^2 g^{-1}), and have a large micro- and mesopore volume (0.75 cm^3 g^{-1}). The carbon aerogels show very promising potential in the separation/extraction of organic pollutants and for energy storage.*

Porous carbon aerogels (CAs) have become highly important owing to their practical value in numerous applications, for example, as adsorption media and catalyst supports and in water treatment, chromatographic separation systems, and energy storage and conversion.[1] Because of their excellent characteristics, such as large specific surface areas (SSAs), controllable porosity, and extraordinary chemical, mechanical, and thermal stability, porous CAs are one of the most competitive materials in these applications when compared to other conventional porous inorganic materials.[2]

However, in many aspects, there is still room for improvement, and countless synthesis methods have been developed. Most CAs are prepared by carbonization of organic precursor aerogels with porous hierarchical structures, such as glucose, fructose, bacterial cellulose (BC), resorcinol–formaldehyde resin (RFR), and phenol–formaldehyde resin (PFR).[3] Organic groups generate micro- or mesopores during carbonization, giving high SSAs. However, almost all of these organic precursor aerogels cannot withstand the capillary force related to the surface tension of the liquid during drying. Thus, in order to avoid the collapse of the micropores, special drying methods, such as supercritical CO_2 drying, are inevitably required.[3d,4] The time-consuming drying process and rigorous drying conditions (especially CO_2 drying) are fatal drawbacks of these methods, which inhibit their wide application. Furthermore, any organic group removed during heat treatment automatically causes a decrease in mass yield and thereby increases the overall price.

The key to success in practical applications strongly depends on inexpensive and convenient large-scale preparation. To further reduce the production cycles and cost, robust polymer aerogels that can withstand capillary pressures and eventually be dried easily, are urgently required. RFR and PFR are one of the most promising precursors owing to the unique microstructures with their inherent, highly cross-linked, rigid structure.[5] The rigid benzene rings and exocyclic sp^3 carbon atoms endow the aerogels with mechanical and thermal stability.[6] However, CAs (RFCAs/PFCAs) derived from normally dried RFR or PFR aerogels (also called xerogel) have high densities (>0.2 g cm^{-3}) and low SSAs (ca. 500 m^2 g^{-1}).[7] Recently, a feasible method was reported for the preparation of porous carbonaceous materials by using glucose in combination with binary salt mixtures during hydrothermal carbonization (HTC).[8] Salts act as porogens and stabilizers, which can be easily washed out with water afterwards, thereby opening up the micropores. The facile and nontoxic hypersaline method represents an alternative green strategy. However, to the best of our knowledge, the preparation of porous CAs by combining the polymerization of monomers and hypersaline conditions has not been reported.

Herein, we have developed a facile, sustainable, and inexpensive route for synthesizing robust PFCAs with a low density of about 25 mg cm^{-3} and a high SSA of 1340 m^2 g^{-1} by applying hypersaline conditions during the polymerization. Special drying methods were no longer required because carbonization and foaming now take place simultaneously, which allows for robustness throughout the whole synthesis procedure. The obtained robust CA can even withstand the surface tension of polar liquids, which allows for drying in a conventional vacuum oven while the nanostructure is retained.

Carbon monoliths were prepared by the polymerization of phenol (P) and formaldehyde (F) under hypersaline con-

[*] Z. L. Yu, G. C. Li, N. Yang, Z. Y. Ma, X. Wang, Prof. Dr. S. H. Yu
Division of Nanomaterials & Chemistry
Hefei National Laboratory for Physical Sciences at the Microscale
Collaborative Innovation Center of Suzhou Nano Science and Technology, Department of Chemistry
CAS Center for Excellence in Nanoscience
Hefei Science Center of CAS
University of Science and Technology of China
Hefei 230026 (China)
E-mail: shyu@ustc.edu.cn
Dr. N. Fechler, Prof. Dr. M. Antonietti
Department of Colloid Chemistry
Max-Planck-Institute of Colloids and Interfaces
Am Mühlenberg 1, 14424 Potsdam-Golm (Germany)
E-mail: Nina.Fechler@mpikg.mpg.de
markus.antonietti@mpikg.mpg.de
Supporting information and the ORCID identification number(s) for the author(s) of this article can be found under: http://dx.doi.org/10.1002/anie.201605510.

 © 2016 Wiley-VCH Verlag GmbH & Co. KGaA, Weinheim

ditions. Two salts, $ZnCl_2$ and NaCl, were selected to examine the effect of hypersaline conditions on the polymerization of P and F as shown in Figure 1. $ZnCl_2$ and NaCl, as two salts with opposing properties, were introduced into the precursor solutions of phenol and formaldehyde. Formalin also served as a dispersant of the salts, and no extra water was added. $ZnCl_2$ could be thoroughly dispersed, forming a homogeneous viscous white slurry (Figure 1a). After the solvothermal polymerization (STP), a stiff homogeneous black PF–$ZnCl_2$ (PZ) monolith was obtained (Figure 1b). In comparison to the original yellow color of pure PFR, this already reveals the strong effect of $ZnCl_2$ on the PFR (Figure S1a).

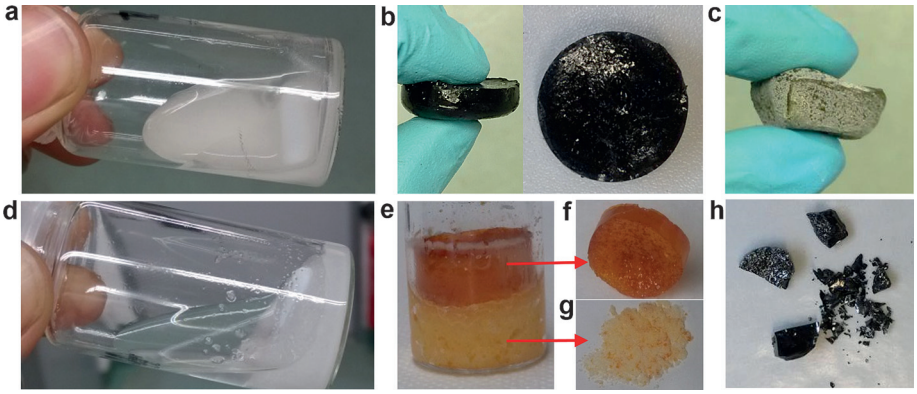

Figure 1. Photographs showing the processing of PFCAs under different hypersaline conditions. a) A mixture of phenol, formaldehyde, and $ZnCl_2$ before STP. b) A PZ monolith after STP. c) A CA after carbonization. d) A mixture of phenol, formaldehyde, and NaCl before STP. e–g) A PS monolith after STP, divided into two parts. h) The PS-derived carbon monolith obtained after carbonization of the monolith shown in (f).

During the carbonization, the PZ monolith expands to several times its original volume because $ZnCl_2$ serves as a dehydration and foaming agent.[9] Finally, $ZnCl_2$ is transformed into ZnO, which was also revealed by the white appearance of the aerogel (Figure 1c; see also the Supporting Information, Figure S2a). After removal of the ZnO by washing with diluted HCl and direct drying in vacuum or in air under ambient conditions, a stable light-weight black CA was obtained (Figure 2a and Figure S2b). The CA is denoted as PZ-*x*-*y*, where *x* indicates the mass of $ZnCl_2$, and *y* indicates the temperature of carbonization. In the case of NaCl, a salting out effect was observed, with phenol floating on the surface and NaCl precipitating at the bottom (Figure 1d). A very hard organic, and afterwards carbon, monolith was obtained from the upper solution aside from a brownish-yellow powder from the NaCl containing phase (Figure 1e–h). It is known that Na^+ is strongly hydrated (a kosmotrope), and therefore, NaCl is also called a "hard salt", thus salting out excess phenol.[8,10] In contrast, soft $ZnCl_2$ acts as a chaotrope and promotes the miscibility of all components. $ZnCl_2$ is thus more suitable than NaCl for generating homogeneous CAs.

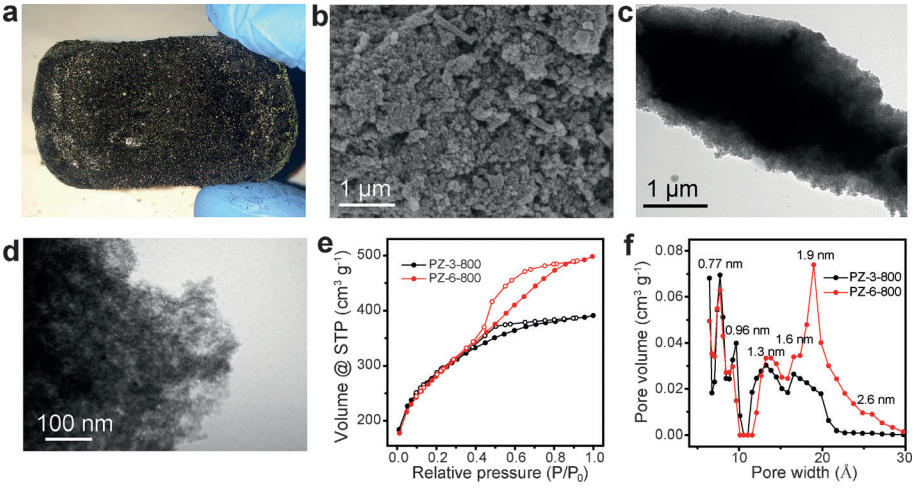

Figure 2. a) Photograph of PZ-6-800 CA. b) SEM and c, d) TEM images showing the microstructure of PZ-6-800. e, f) Nitrogen sorption isotherms and pore size distributions of PZ-3-800 and PZ-6-800.

The mass of $ZnCl_2$ has a strong influence on the morphology of the PZ monolith (Figure S3), and a homogeneous black PZ monolith can only be obtained in a suitable mass range ($3\,g \le ZnCl_2 \le 6\,g$ for the typical synthesis with 0.01 mol phenol). Too low amounts of $ZnCl_2$ will induce phase separation because the conditions are no longer hypersaline, which leads to inhomogeneities in the light-colored monolith (Figure S3, entry 2). Thus it barely influences the monolith if the $ZnCl_2$ amount is further reduced (Entry 1). On the other hand, when the $ZnCl_2$ content is too high, the mixed phase is not liquid anymore, and water is needed to dissolve the excess $ZnCl_2$ (Figure S3, entry 4).

After vacuum drying and thermal treatment in an inert-gas oven, the as-obtained PZ-6-800 CA was purified simply by washing with HCl followed by vacuum drying (Figure 2a). It should be noted that the nanostructure of the CA is unusually robust so that it is not necessary anymore to employ freeze drying or supercritical CO_2 drying to circumvent the collapse of the micropores that is triggered by capillary forces. The nanostructure of PZ-6-800 CA was analyzed by scanning electron microscopy (SEM) and transmission electron microscopy (TEM; Figure 2b–d), which revealed the carbon material to be composed of fine interconnected carbon frazzles of about 10 nm. In contrast, conventional syntheses of PF-derived carbon materials without any salt only result in dense structures (Figure S4). This underlines the role of the $ZnCl_2$, which acts as a surface stabilizer and dispersant.

© 2016 Wiley-VCH Verlag GmbH & Co. KGaA, Weinheim

For detailed porosity analysis, nitrogen sorption measurements were carried out to determine the apparent surface areas and pore size distributions by applying the Brunauer–Emmett–Teller (BET) model and the nonlocal density functional theory (NLDFT) equilibrium model for slit pores, respectively (Figure 2e,f). The surface areas of PZ-3-800 and PZ-6-800 are both close to 1300 $m^2 g^{-1}$, and thus much higher than those of conventional PFCAs (ca. 700 $m^2 g^{-1}$).[11] Detailed analysis of the low-pressure region revealed a high number of micropores with diameters from 0.77 to 1.6 nm (Figure 2f). Increasing the amount of $ZnCl_2$ did not increase the SSA or lead to more micropores but introduced more mesopores with diameters of 1.9 nm and 2.6 nm. This is consistent with the hysteresis loop in the sorption isotherm of PZ-6-800 (Figure 2e,f). The monolith made with NaCl was labeled PS-*x*-*y*, in accordance with the above-mentioned nomenclature. PS-6-800 is a very dense carbon monolith with practically no SSA, which was also revealed by the smooth surfaces, indicating the nonporous nature (Figure S5a,b). This underlines the fact that the porosity of the CAs indeed mainly depended on the nature of the salt. A pure PF monolith of bright yellow color that was synthesized without any salts served as an internal standard (Figure S1a). The carbonized PF (PF-800) did not possess any substantial SSA owing to the inherently dense nature of this conventional system (Figure S1b,c). SEM and TEM images show the smooth surface and dense structure of PF-800, which is similar to that of PS-6-800 (Figure S4a,b).

To obtain further insight into the formation of the hypersaline carbon monoliths, the material before carbonization was analyzed. Being very different from the dense pure PF monoliths, the black PZ-6 monolith obtained after polymerization under hypersaline conditions could be permeated and washed with HCl. This already indicates that a porous structure was formed during the STP process, which was accompanied by a color change into khaki (Figure S6a,b). The washed PZ-6 (WPZ-6) has a less dense microstructure than PZ-6, which is composed of bigger granules (Figure S6c,d). Keeping in mind that the monolith was only dried in simple vacuum, WPZ-6 has an improved SSA compared to the undetectable SSA of PZ-6 (Table S1). Thus $ZnCl_2$ has a powerful influence on the microstructure of the monolith. Fourier transform infrared spectroscopy (FTIR) was used to illustrate the differences between PF and WPZ-6 monoliths. As shown in Figure S7, PF gives rise to strong bands at about 1474 and 1200 cm^{-1}, which are due to the scissoring vibrations of $-CH_2-$ and C–OH, respectively. (Characteristic signals include the phenolic and aliphatic OH band at ca. 3438 cm^{-1}, the methylene $-CH_2-$ peak at 2913 cm^{-1}, the –C=O band at 1648 cm^{-1}, the aromatic C=C band at 1605 cm^{-1}, and the C–OH band at 1200 cm^{-1}.)[12] The introduction of $ZnCl_2$ strongly weakens the $-CH_2-$ bands at approximately 1474 and 2913 cm^{-1}, but enhances the aromatic C=C band, indicating that $ZnCl_2$ can facilitate dehydrogenation and aromatization. Furthermore, the OH band at about 3438 cm^{-1} became narrow and was blue-shifted to about 3574 cm^{-1}; this was accompanied by the weakening of the aliphatic OH band (1200 cm^{-1}) and the disappearance of the –C=O band (1648 cm^{-1}), illustrating the deoxygenation effect of $ZnCl_2$. However, this process seems to be reversible as the bands were recovered after washing. ^{13}C NMR spectroscopy was performed to further reveal the structure differences caused by $ZnCl_2$ (Figure S8). Two clear resonances at about 180 and 20 ppm, corresponding to carbonyl and methyl groups, respectively, are visible for PZ-6 and are still observed even after washing; they were, however, not found for the pure PF. The addition reaction of phenol and formaldehyde to active hydroxymethyl and the further dehydration condensation reaction constitute the whole polymerization reaction of PF. Thus the carbonyl and methyl groups are most likely formed during the deoxygenation and dehydrogenation of hydroxymethyl in the presence of $ZnCl_2$. Eventually, $ZnCl_2$ can facilitate the dehydration and carbonization of the phenolic resin during the STP process.

To reveal the origin of the high SSA and pore volume, the same carbonization procedure was conducted with WPZ-6, as shown in Figure S6e,f. The WPZ-6-derived CA (WPZ-6-800) has a much higher SSA (660 $m^2 g^{-1}$) and pore volume (0.24 $cm^3 g^{-1}$) than pure PF-800 (ca. 5 $m^2 g^{-1}$). Its micropores with diameters of 0.5–0.6 nm display a narrow size distribution (Figure S6f). The residual zinc content in WPZ-6–800 is negligible (0.0054 wt%) as measured by inductively coupled plasma mass spectroscopy (ICP-MS), which means that the salt is essentially washed away before carbonization. Thus $ZnCl_2$ obviously plays a key role in the formation of the porous microstructure already from the very beginning, that is, during the polymerization. Here, the modified microstructure contributes about 51% of the SSA of PZ-6-800 CA. The rest is probably based on the dehydration effect of $ZnCl_2$ and the derived ZnO nanocrystals, resulting in a pore size distribution of 0.77–1.6 nm (Figure 2f).

Elemental analysis was conducted to investigate the effect of $ZnCl_2$ on the composition of the carbon materials. The monolith WPZ-6, which was polymerized in the presence of salt, has a much lower oxygen content (ca. 10.83 wt%) and a higher C/O ratio than pure PF (ca. 16.55 wt%), which also supports the deoxygenation effect of $ZnCl_2$ (Table 1 and Table S1). After carbonization, the O content of PZ-6-800 significantly decreased to only 5.54 wt% compared to 11.30 wt% in pure PF-800. $ZnCl_2$ efficiently causes deoxygenation at high temperatures by removing oxygen in the form of water, but also by carbothermal reduction. The deoxygenation greatly depends on the amount of $ZnCl_2$ (8.18 wt% in

Table 1: Elemental compositions, surface areas, and pore volumes of the materials.

Sample	SSA [$m^2 g^{-1}$]	Pore volume [$cm^3 g^{-1}$]	Elemental analysis (wt%) C	O
pure PF	0	0.00	74.36	16.55
WPZ-6	10	0.02	76.34	10.83
PF-800	5	0.00	87.48	11.30
WPZ-6-800	660	0.24	87.90	10.76
PF/$ZnCl_2$-800	730	0.65	93.00	5.43
PZ-3-800	1300	0.56	91.30	8.18
PZ-6-800	1300	0.72	93.34	5.54
PS-3-800	0	0.00	88.24	10.90

 © 2016 Wiley-VCH Verlag GmbH & Co. KGaA, Weinheim

PZ-3-800). Contrary to the positive effect of $ZnCl_2$, NaCl has a negligible effect as PS-3-800 showed no differences to PF-800 in terms of both the microstructure and the elemental composition. To further reveal the effect of hypersaline conditions on the polymerization, pure PFR was thoroughly mixed with $ZnCl_2$ in the same mass ratio as PZ-6 and then carbonized, similarly to the previous works on carbon powders where $ZnCl_2$ was added to commercial resol.[9] Because of the stiff nature of the PF monoliths, ball milling was necessary to ensure thorough mixing. The obtained carbon powder is referred to as PF/$ZnCl_2$-800 and exhibits almost the same elemental composition as PZ-6-800, but a much lower SSA (730 $m^2 g^{-1}$; Figure S9). These results reveal that the pore generation during the hypersaline synthesis route is very different from mechanical post-treatment, that is, the salt has a direct influence on the polymerization (Table 1).

We found that ZnO can also be simply removed just by heating to higher temperatures, here 900 °C. Indeed, the ZnO content of PZ-6-900 was reduced even compared to that of PZ-6-800. After heat treatment for two hours, almost no residual ZnO was detected by XRD (Figure S10a). ICP analysis also confirmed the zinc content of PZ-6-900 to be almost negligible (< 0.01 wt %) compared to that of PZ-6-800 (0.17 wt %), which is washed with HCl. Eventually, high-temperature evaporation is more efficient and time-saving than HCl washing in removing ZnO. The obtained lightweight PZ-6-900 CA has a low density of about 25 mg cm^{-3} (Figure S10b), which is much lower than those of previously described PFCAs and RFCAs.[7b,13] Similar to PZ-6-800, PZ-6-900 CA also displays a high SSA of approximately 1340 $m^2 g^{-1}$ and a large micropore volume of 0.75 $cm^3 g^{-1}$ (Figure S11). Because of the carbothermal reduction and subsequent evaporation of the Zn, no further washing is needed, which renders the whole process even more convenient.

The CA (PZ-6-900) can float on the surface of water owing to its hydrophobicity and lightweight construction (Figure 3a); however, it plunges into organic solvents such as ethanol and *n*-hexane owing to the capillary uptake of hydrophobic liquids. PFCA exhibits a very high absorption capacity for common organic solvents and physically stores the organic molecules (Figure 3b). The weight absorption capacity increases nearly linearly with the density of the organic solvent, which means that always the same volume is stored (Figure S12). The lipophilicity and high porosity (ca. 98.6 %) ensure that PFCAs are potential candidates for the efficient separation and extraction of organic pollutants or oils.

As for recycling, many carbon-based absorbents are often recovered by burning off the organic solvent, which is a waste of energy and organic solvent.[3c] Feasible routes to recycle absorbates include the squeezing of highly compressible absorbents such as expanded graphite and vacuum filtration; however, both approaches can only retrieve 70 % of the adsorbates.[14] Owing to its robust structure, PFCA is an ideal absorbent for organic solvents, which can be retrieved by distillation or mild heat treatment. Here, we chose ethanol and *n*-hexane as examples for common polar and nonpolar

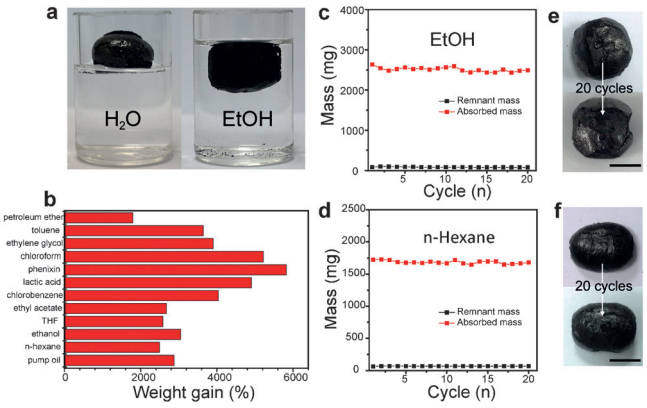

Figure 3. a) Photographs showing the hydrophobicity of PZ-6-900 CAs. b) Absorption efficiency of PZ-6-900 CAs towards commonly used organic solvents. c, d) Recyclability of PZ-6-900 CAs for ethanol (c) and *n*-hexane (d) absorption and release upon heat treatment (100 °C) for 20 cycles. e, f) Photographs showing the differences in sample size after 20 cycles. The PFCAs maintained their original size and showed almost no shrinkage.

solvents, respectively. Vacuum drying at high temperature (100 °C) above the boiling point was conducted to simulate the heat treatment process. The residual mass was then determined until it was constant. The recyclability of the PFCA and the recoverability of the adsorbates were examined by repeating the process 20 times. As shown in Figure 3c and d, after 20 cycles, there is no obvious fading of the absorption capacity. 99.5 % of the ethanol and 99.7 % of the *n*-hexane could be extracted in the first cycle (Figure 3c, d). Furthermore, the PFCAs maintained their original macroscopic size and showed no shrinkage after 20 cycles (Figure 3e, f). This demonstrates that the microstructure is robust enough to withstand the surface tension and treatment process many times.

Owing to the high SSA (1300 $m^2 g^{-1}$), high micropore volume (0.72 $cm^3 g^{-1}$), and high transport pore content, PFCAs are also a promising electrode material for lithium ion batteries (LIBs). As shown in Figure S13, PZ-6-800 was selected as an example to examine the performance as a negative electrode material in LIBs. At 0.1 A g^{-1}, it provided a reversible charging capacity of 798.2 mA h g^{-1}, albeit with a high initial discharge capacity of 1680.5 mA h g^{-1}. This means that 50 % of the initial charge is used to build up the solid electrolyte interface layer. After 100 cycles, a high capacity of 427 mA h g^{-1} still remained, confirming the favorable cyclability. As the current density was gradually increased from 0.1 to 2 A g^{-1}, the anode delivered a stable electrochemical performance, indicating excellent high-rate stability (Figure S13b, c). To further examine the practicality of this material as an anode for long-lifetime LIBs, extended cycling tests at a current density of 1 A g^{-1} were performed. Even at these high rates, the material displayed a high specific capacity of 300 mA h g^{-1} after 1000 cycles with a Coulomb efficiency (CE) of nearly 100 % (Figure S13d). The slight increase in the specific capacity after 700 cycles may be caused by electrochemical activation during the charge–discharge process. The good performance demonstrates that

© 2016 Wiley-VCH Verlag GmbH & Co. KGaA, Weinheim

the PFCAs, after some chemical adaption to minimize the primary capacity loss, can be turned into promising candidates for metal anode applications.

In conclusion, a facile route to unusually robust CAs with a low density of about 25 mg cm^{-3} and a high SSA of approximately 1340 m^2 g^{-1} was developed that is based on simple polymerization of PF under hypersaline conditions. $ZnCl_2$ was used as dehydrating agent, stabilizer, and porogen, and crucial to directly obtain the stable PFCAs. Special drying methods could be avoided during the whole synthesis process as the usually very delicate organic aerogels were robust from the beginning. The simultaneous carbonization and foaming process of the dense PF monoliths kept the structure stable even throughout carbon formation. The obtained robust CAs can withstand even the capillary pressure of polar liquids, allowing for drying under ambient or vacuum conditions. The highly porous PFCAs could also be obtained without any washing step by making use of an advantageous carbothermal reduction/evaporation process. We believe that this facile, low-cost, and scalable synthesis will promote further practical use of PFCAs while their properties can be fine-tuned in accordance with the desired application, for example, for the separation or extraction of organic pollutants or oils and energy storage.

Acknowledgements

We acknowledge the funding support from the National Natural Science Foundation of China (Grant 21431006), the Foundation for Innovative Research Groups of the National Natural Science Foundation of China (Grant 21521001), the National Basic Research Program of China (Grants 2014CB931800, 2013CB931800), the Users with Excellence and Scientific Research Grant of Hefei Science Center of CAS (2015HSC-UE007, 2015SRG-HSC038), and the Chinese Academy of Sciences (Grant KJZD-EW-M01-1).

Keywords: carbon aerogels · hypersaline conditions · phenol–formaldehyde resin · porosity · zinc dichloride

How to cite: *Angew. Chem. Int. Ed.* **2016**, *55*, 14623–14627
Angew. Chem. **2016**, *128*, 14843–14847

[1] a) G. P. Hao, W. C. Li, D. Qian, G. H. Wang, W. P. Zhang, T. Zhang, A. Q. Wang, F. Schüth, H. J. Bongard, A. H. Lu, *J. Am. Chem. Soc.* **2011**, *133*, 11378–11388; b) Z. Chu, Y. Feng, S. Seeger, *Angew. Chem. Int. Ed.* **2015**, *54*, 2328–2338; *Angew. Chem.* **2015**, *127*, 2358–2368; c) J. Liang, X. Du, C. Gibson, X. W. Du, S. Z. Qiao, *Adv. Mater.* **2013**, *25*, 6226–6231; d) X. Yang, C. Cheng, Y. Wang, L. Qiu, D. Li, *Science* **2013**, *341*, 534–537; e) S. Xin, Y.-G. Guo, L.-J. Wan, *Acc. Chem. Res.* **2012**, *45*, 1759–1769.

[2] a) N. Fechler, T. P. Fellinger, M. Antonietti, *Adv. Mater.* **2013**, *25*, 75–79; b) T.-P. Fellinger, A. Thomas, J. Yuan, M. Antonietti, *Adv. Mater.* **2013**, *25*, 5838–5855; c) T. Yang, J. Liu, Y. Zheng, M. J. Monteiro, S. Z. Qiao, *Chem. Eur. J.* **2013**, *19*, 6942–6945; d) M. Antonietti, N. Fechler, T.-P. Fellinger, *Chem. Mater.* **2014**, *26*, 196–210.

[3] a) H. W. Liang, Q. F. Guan, L. F. Chen, Z. Zhu, W. J. Zhang, S. H. Yu, *Angew. Chem. Int. Ed.* **2012**, *51*, 5101–5105; *Angew. Chem.* **2012**, *124*, 5191–5195; b) S. Kubo, R. J. White, K. Tauer, M.-M. Titirici, *Chem. Mater.* **2013**, *25*, 4781–4790; c) Z. Y. Wu, C. Li, H. W. Liang, J. F. Chen, S. H. Yu, *Angew. Chem. Int. Ed.* **2013**, *52*, 2925–2929; *Angew. Chem.* **2013**, *125*, 2997–3001; d) S. A. Al-Muhtaseb, J. A. Ritter, *Adv. Mater.* **2003**, *15*, 101–114.

[4] A. M. Elkhatat, S. A. Al-Muhtaseb, *Adv. Mater.* **2011**, *23*, 2887–2903.

[5] a) X. Wang, L. L. Lu, Z. L. Yu, X. W. Xu, Y. R. Zheng, S. H. Yu, *Angew. Chem. Int. Ed.* **2015**, *54*, 2397–2401; *Angew. Chem.* **2015**, *127*, 2427–2431; b) Z.-L. Yu, Z.-Y. Wu, S. Xin, C. Qiao, Z.-Y. Yu, H.-P. Cong, S.-H. Yu, *Chem. Mater.* **2014**, *26*, 6915–6918.

[6] K. Ai, Y. Liu, C. Ruan, L. Lu, G. Lu, *Adv. Mater.* **2013**, *25*, 998–1003.

[7] a) D. Wu, R. Fu, S. Zhang, M. S. Dresselhaus, G. Dresselhaus, *Carbon* **2004**, *42*, 2033–2039; b) A. Léonard, N. Job, S. Blacher, J.-P. Pirard, M. Crine, W. Jomaa, *Carbon* **2005**, *43*, 1808–1811.

[8] N. Fechler, S.-A. Wohlgemuth, P. Jäker, M. Antonietti, *J. Mater. Chem. A* **2013**, *1*, 9418.

[9] Z. Yue, C. L. Mangun, J. Economy, *Carbon* **2002**, *40*, 1181–1191.

[10] L. M. Pegram, M. T. Record, *J. Phys. Chem. B* **2007**, *111*, 5411–5417.

[11] a) T. Horikawa, J. i. Hayashi, K. Muroyama, *Carbon* **2004**, *42*, 1625–1633; b) H. Tamon, H. Ishizaka, T. Araki, M. Okazaki, *Carbon* **1998**, *36*, 1257–1262.

[12] a) Y. Zhang, S. Shen, Y. Liu, *Polym. Degrad. Stab.* **2013**, *98*, 514–518; b) D.-D. Guo, M.-S. Zhan, K. Wang, *J. Appl. Polym. Sci.* **2012**, *126*, 2010–2016.

[13] a) R. Zhang, Y. Lu, L. Zhan, X. Liang, G. Wu, L. Ling, *Carbon* **2003**, *41*, 1660–1663; b) R. Brandt, R. Petricevic, H. Probstle, J. Fricke, *J. Porous Mater.* **2003**, *10*, 171–178.

[14] a) H. Bi, X. Xie, K. Yin, Y. Zhou, S. Wan, L. He, F. Xu, F. Banhart, L. Sun, R. S. Ruoff, *Adv. Funct. Mater.* **2012**, *22*, 4421–4425; b) H. Bi, Z. Yin, X. Cao, X. Xie, C. Tan, X. Huang, B. Chen, F. Chen, Q. Yang, X. Bu, X. Lu, L. Sun, H. Zhang, *Adv. Mater.* **2013**, *25*, 5916–5921; c) H. Bi, X. Huang, X. Wu, X. Cao, C. Tan, Z. Yin, X. Lu, L. Sun, H. Zhang, *Small* **2014**, *10*, 3544–3550; d) H. Hu, Z. Zhao, Y. Gogotsi, J. Qiu, *Environ. Sci. Technol. Lett.* **2014**, *1*, 214–220.

Received: June 6, 2016
Revised: July 5, 2016
Published online: September 8, 2016

 © 2016 Wiley-VCH Verlag GmbH & Co. KGaA, Weinheim